5

Results

5.1 *Static speckle patterns*

Fig. 5.1 shows an image of a speckle pattern of Cu_3Au, measured with $D = 7.5\ \mu$m. The sample was kept at room temperature where the dynamics is frozen. The data are characterized by three well separated length scales: the speckle size and the domain sizes. It is well known that Cu_3Au superlattice peaks are disks in reciprocal space (See section 2.4). In the far field diffraction plane, regions of high intensity are next to regions of low intensity, with a typical speckle size of l_s, which is on the order of the FWHM of the Fraunhofer diffraction pattern of the pinhole given by [15]

$$l_s \approx \frac{1.0288\lambda R_d}{D}. \tag{5.1}$$

Here $R_d = 1.04$ m is the pinhole-detector distance, $\lambda = 1.797$ Å and D is the input beam collimator diameter. The speckle angular size is given by a relative change of optical path length equal to λ[15]. Here, l_s is 25 μm or approximately a pixel wide. Note also that for a *perfectly coherent* incident beam, the speckle size goes to zero in the limit where the scattering volume goes to infinity. Therefore, it is possible to wash out the contrast if the speckle size becomes smaller than the resolution of the detector. It is important to match the detector resolution with the speckle size.

In the far field diffraction, the speckle pattern adds a random fluctuating envelope to the (100) superlattice peak caused by coherent diffraction from X-rays scattered from different antiphase domains. They are called antiphase domains because type I and II domains walls cause π phase shifts in the scattered light from the (100) since these walls are created by a relative displacement of (1/2,0,1/2)a, where a is the lattice

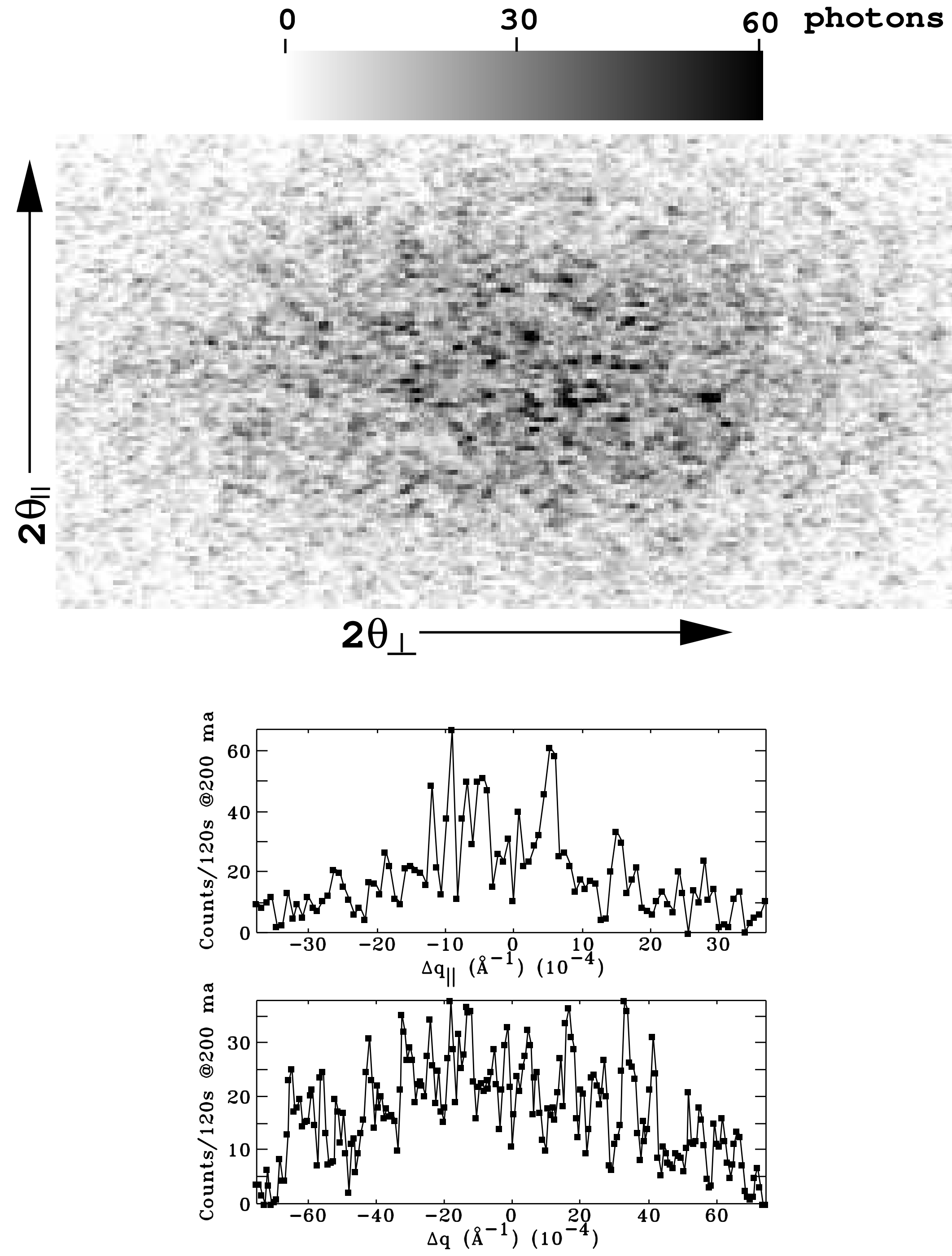

Figure 5.1: A speckle pattern of Cu_3Au (100) measured at room temperature after the sample was ordered for 16 h at $373°C$. The scattered intensity in the central 200×100 pixels is displayed using the grey scale legend. The beam was collimated with a 7.5 μm pinhole and the pattern was integrated for 2 minutes. The data are scaled for beam intensity decay to a beam current of 200 mA. Below, two slices are shown, one along $2\Theta_{\|}$ with $\vec{\Delta q} = (0, \Delta q_{\|})$ and one along $2\Theta_{\perp}$ with $\vec{\Delta q} = (\Delta q_{\perp}, 0)$. The error bars are given by approximately $\sqrt{1.63v^*}$, as shown in Fig 3.6. To reduce the error bars, several scans can be averaged (see Fig 5.2). The spatial fluctuations are clearly above counting statistics.

constant. The superlattice peak characteristic angular size $\Delta \approx \lambda R_d / R_D$, where R_D is the average radius of an antiphase domain in Cu_3Au. In Fig. 5.1, Δ is of the order of 30 to 60 pixels, therefore the average domain size ranges from 1400 to 2800 Å. The optimum condition for observing speckle occurs when Δ is of the order of a few l_s so that the number of speckles measured by the CCD is of the order of $(D/R_D)^2$. When $R_D > D$, one simply observes the Fraunhofer pattern of the pinhole because the sample has no disorder. This was observed in Ref. [15] on a perfect crystal of Si. If the diffuse scattering is too broad, more speckles are observed, but the scattered intensity is smaller. With current X-ray sources, one must prepare samples carefully to observe speckle. Future third generation synchrotron sources should allow for a greater variety of samples to be studied.

Another characteristic property of speckle is its very large contrast, defined as the ratio of the standard deviation of the spatial fluctuations over the spatial average. The contrast depends on two experimental conditions: the incident beam resolution and the detector resolution. A large number N_s of independent speckles in a detector area reduces the contrast by a factor $1/\sqrt{N_s}$ for a perfectly coherent incident beam. Approximating the speckle area, A_s, by a disk of radius equal to the first zero of the Fraunhofer diffraction pattern of the pinhole,

$$A_s = \pi \left(\frac{1.22 \lambda R_d}{D} \right)^2 , \tag{5.2}$$

one finds the number of speckles in a detector area A_d

$$N_s = \frac{A_d}{A_s} = \frac{A_d D^2}{\pi (1.22 \lambda R_d)^2} . \tag{5.3}$$

Since $N_s \propto D^2$, the contrast is proportional to $1/D$ for a fixed detector area, thus increasing the pinhole diameter reduces the contrast.

The incident beam resolution is related to the degree of coherence of the beam, measured by the ratio of the beam size over the transverse coherence lengths l_x, l_y. Here, the sample size is controlled by the collimating pinhole diameter D. Increasing l_x,l_y or reducing D improves the contrast. A useful parameter for determining the contrast is the number of coherence areas $A_c = l_x l_y$ in the collimating pinhole area given by

$$N_c = \frac{\pi D^2}{4 l_x l_y}. \tag{5.4}$$

The contrast increases as N_c decreases.

To demonstrate these concepts, we performed an experiment which consisted of changing l_x and D independently. The horizontal transverse coherence length l_x was increased by closing the source x-y slits, thus reducing the effective source size d_s (See Fig 2.4). Only l_x was changed because the horizontal source size of synchrotron radiation is typically an order of magnitude larger than the vertical source size, resulting in l_x being the smallest of the two coherence lengths.

Fig. 5.2 shows slices of the speckle pattern for different D and source sizes. This experiment was performed at X-25, with a ring current ranging from 210 to 150 mA. The CCD was oriented at the time with its poor resolution direction along $2\Theta_{||}$. The horizontal source size was reduced by closing the upstream slits which are 10.5 m from the source, from an opening of 2 mm to 0.31 mm. This reduced the incident intensity by approximately 2/3. The CCD was exposed for 30 to 240 s. To improve the counting statistics, many scans were averaged for a total time ranging from 20 minutes to an hour. Slices through the time averages along $2\Theta_{\perp}$ and $2\Theta_{||}$ are shown. As expected theoretically, the speckle pattern spatial fluctuations increase as D is reduced while keeping l_x constant, and are increased when the source size is reduced keeping D constant. The error bars are much smaller that the spatial fluctuations of the signal for all optical conditions. This will be shown later with Fig 5.9. Note that here the peak average count rate is proportional to the pinhole area and slit opening. The contrasts along both scan directions are very similar. Some of the scans along $2\Theta_{||}$ may have less contrast than their respective scans along $2\Theta_{\perp}$ because the CCD resolution is poorer along this direction.

Fig 5.1 and 5.2 show that the contrast and speckle size of the observed speckle pattern are qualitatively consistent with the theoretical properties of speckle. To measure these properties quantitatively, in the next two sections we develop tools which will help to measure the contrast and speckle size of a given speckle pattern.

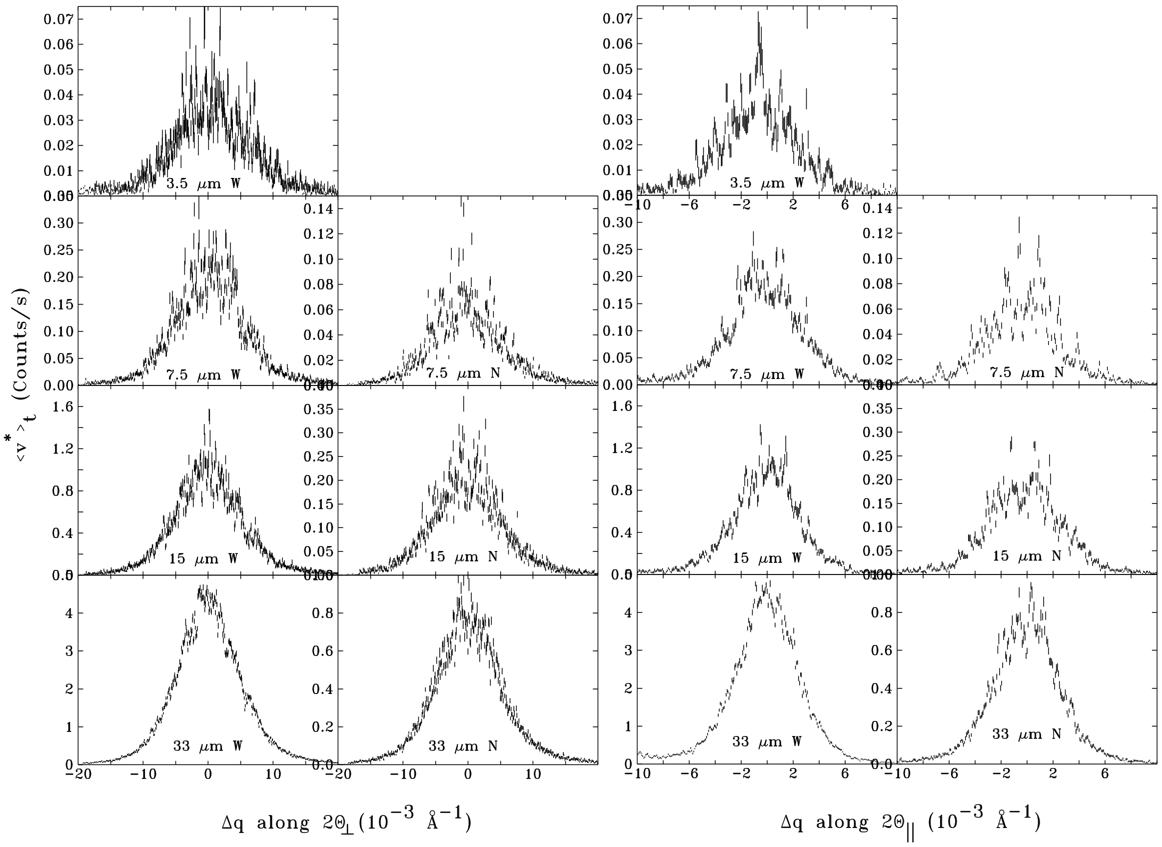

Figure 5.2: Slices along $2\Theta_\perp$ and $2\Theta_{||}$ of the time averaged speckle pattern of Cu_3Au (100) at 300 K, where no coarsening dynamics is expected. The labels indicate the pinhole diameter used and status of the upstream slits: narrow (N) or wide (W). The setup with $D = 3.5$ μm and narrow slits was not measured because of the long integration time needed. The error bars were calculated from Eq. A.14 using the measured variance of N exposures. As discussed in the text, the contrast is reduced when the diameter of the collimating pinhole D is increased at constant incident source size, and is increased by reducing the source size at constant D. Scans along $2\Theta_\perp$ and $2\Theta_{||}$ have very similar contrasts.

These tools could not be used as effectively without a two dimensional data set. This is the main advantage of measuring speckle patterns with a CCD. Here, one can calculate different statistical estimators which describe quantitatively the speckle pattern properties. These estimators will have excellent statistics because the CCD records 2.2×10^5 pixel elements simultaneously, compared to one element for a standard detector. For example, Fig 5.1 would have taken 666 hours of valuable synchrotron beam time to record by scanning a scintillation counter over the same area, or 3.3 hours by scanning a 25 μm slit in front of the one-dimensional linear diode array discussed earlier in section 3.0.4.

5.1.1 Measuring speckle size

To quantify the three length scales of speckle patterns, we will use a more general form of the spatial correlation introduced earlier in Eq. 3.21. The crosscorrelation function of the scattered X-rays is defined[1] by

$$\Gamma(\vec{\Delta q}, t, \Delta t) \equiv < v^*(\vec{q}, t) v^*(\vec{q} + \vec{\Delta q}, t + \Delta t) >_{\vec{q}} . \tag{5.5}$$

The linearized signal v^*, defined in Eq. 3.20, is measured at wavevector $\vec{q}$ and time t, where q_{ij} and t_k are discrete due to the nature of the detection process. The integers i and j are indexes for the rows and columns of the CCD; v^* is integrated from t to $t+\tau$. Let us first understand the autocorrelation function by setting Δt to zero. An image of $\Gamma(\vec{\Delta q}, t, 0)$ is shown in Fig. 5.3 for a typical speckle pattern measured with a 7.5 μm pinhole. Two perpendicular slices of Γ are also shown in Fig. 5.4. The autocorrelation consists of two peaks with well separated length scales. One peak has a width of the order of tens of pixels, caused by the envelope of scattering previously discussed. The central peak is related to the speckle pattern convolved with the detector's response autocorrelation. As shown in the inset of Fig. 5.4 and the enlarged central peak area in Fig 5.3, the scattering is well correlated on a distance of 1-2 pixels.

[1] It is calculated numerically by $\Gamma(\vec{\Delta q}, t, \Delta t) = fft^{-1}(fft(v(t)) fft^*(v(t+dt)))$, where the fft is a spatial Fast Fourier Transform. It can be calculated also directly by evaluating the sums described on page IX. Both methods are equivalent.

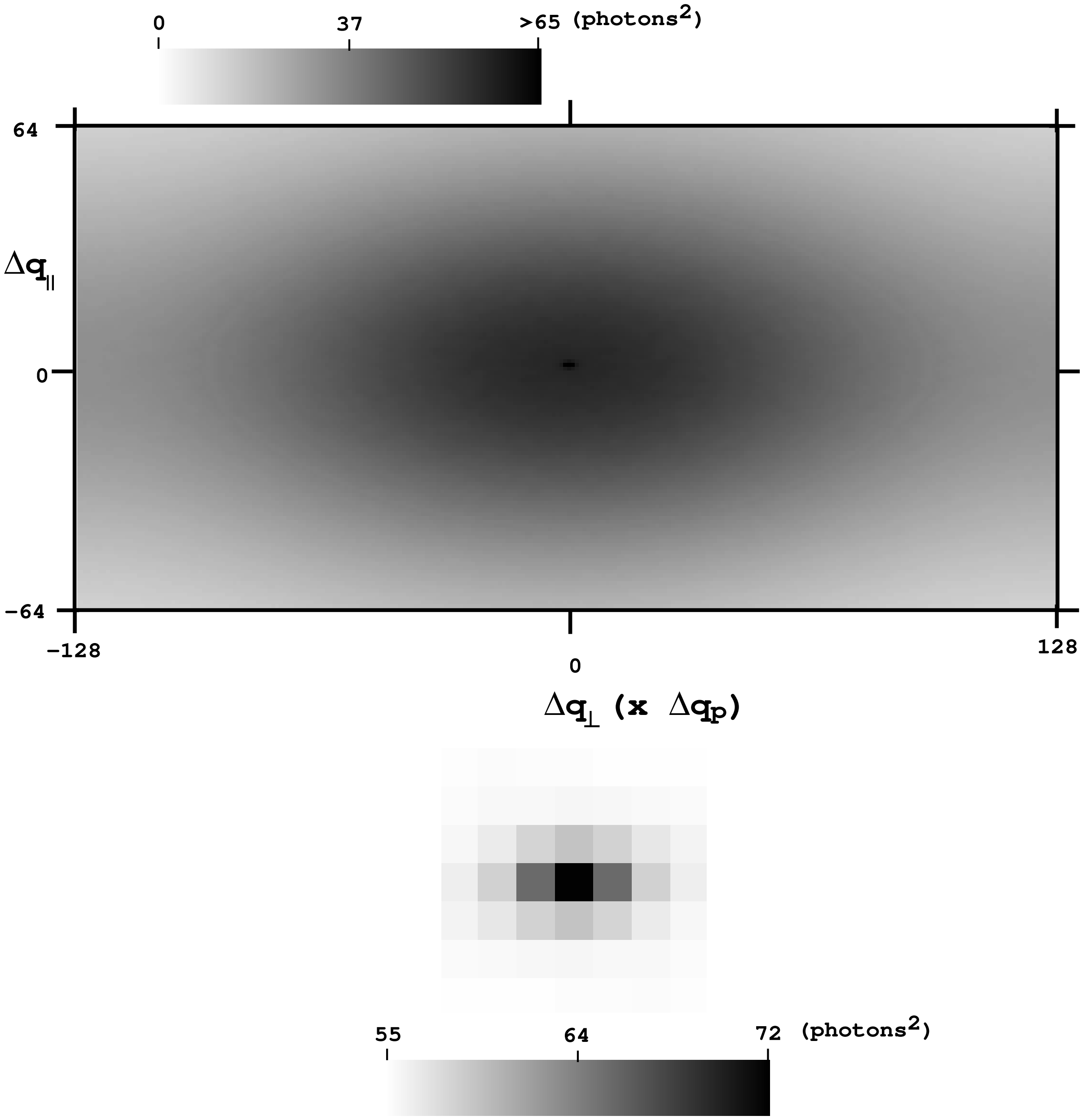

Figure 5.3: A typical autocorrelation function $\Gamma(\vec{\Delta q}, t, 0)$ of the (100) superlattice peak of Cu_3Au. A linear grey scale between 0 and 65 photons^2 is used for displaying Γ, and a pixel subtends a $\Delta q_p = 7.53 \times 10^{-5}$ Å. Below, the central 7×7 pixels of Γ with its color legend. The central peak is related to the speckle size convolved with the detector pixel to pixel correlation.

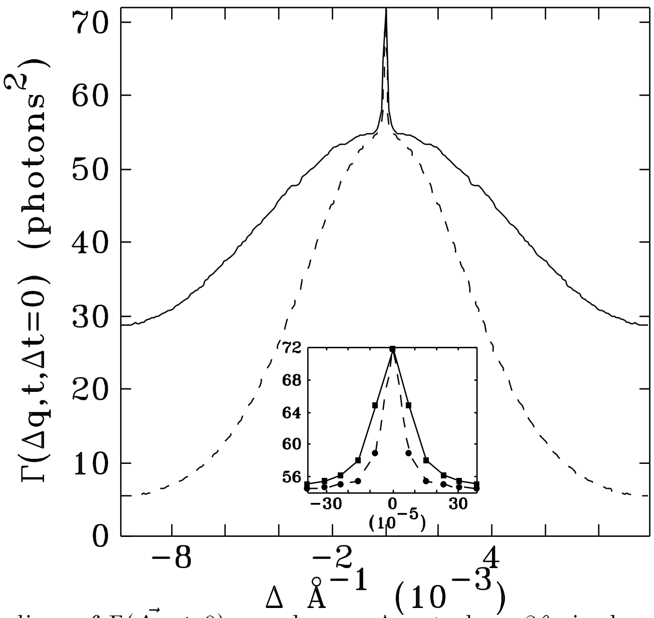

Figure 5.4: Two slices of $\Gamma(\vec{\Delta q}, t, 0)$ are shown. A cut along $2\theta_{\parallel}$ is shown with a dashed line with $\vec{\Delta q} = (0, \Delta)$, and a cut along $2\theta_{\perp}$ with $\vec{\Delta q} = (\Delta, 0)$ is displayed with a solid line. The width of the diffraction pattern is about twice as narrow along $2\theta_{\parallel}$. This difference is explained in section 2.4, where it is shown that the structure factor is pancake-like in reciprocal space. The inset shows the peak near $\vec{\Delta q} \approx 0$. The width of the peak is narrower along $2\theta_{\parallel}$ because the detector resolution is better in this direction. Note that the autocorrelation is symmetric with respect to the origin by definition.

To understand $\Gamma(\vec{\Delta q}, t, 0)$ quantitatively, let us first illuminate the detector with a spatially uniform source of incoherent X-rays with spatial average $<v^*>_{\vec{q}}$. We have shown in section 3.0.5, Fig 3.10, that

$$\Gamma_D(<v^*>, \vec{\Delta q}) - <v^*>^2_{\vec{q}} \approx \begin{cases} 1.63<v^*>_{\vec{q}}, & \text{for } \vec{\Delta q} = 0, \\ 0.85<v^*>_{\vec{q}}, & \text{for } \vec{\Delta q} = (\Delta q_p, 0), \\ 0.2<v^*>_{\vec{q}}, & \text{for } \vec{\Delta q} = (0, \Delta q_p), \\ 0.13<v^*>_{\vec{q}}, & \text{for } \vec{\Delta q} = (2\Delta q_p, 0), \\ 0.11<v^*>_{\vec{q}}, & \text{for } \vec{\Delta q} = (\pm\Delta q_s, \pm\Delta q_p), \\ 0 & \text{otherwise.} \end{cases} \tag{5.6}$$

Here Δq_p is the magnitude of the wavevector difference between two nearest neighbor pixels. Using $S^2_{v^*,\vec{q}} \approx 1.63<v^*>_{\vec{q}}$, it is easy to derive Eq. 5.6 from Eq. 3.21. The detector autocorrelation Γ_D is due to the spreading of the electric charge from a detected photon over several pixels. Fig. 5.5 and 3.10 show slices along $q_{\perp}$ and $q_{\parallel}$ of Γ_D for a spatially uniform detected beam. The CCD has a narrower resolution

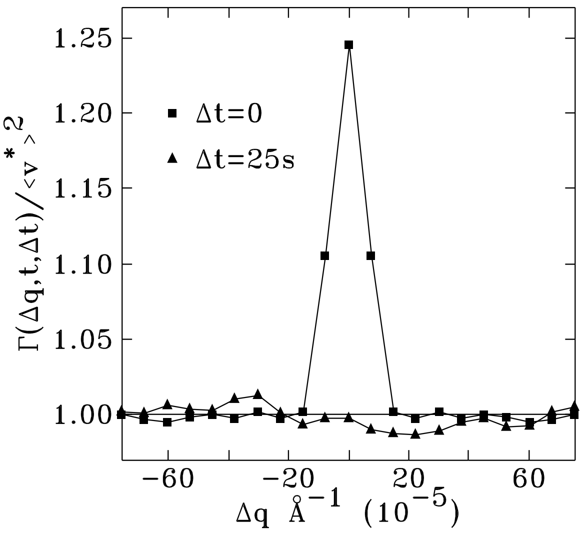

Figure 5.5: With squares, a typical slice of the autocorrelation function $\Gamma_D = <v^*(\vec{q},t)v^*(\vec{q}+\vec{\Delta q},t+\Delta t)>_{\vec{q}}$ for $\Delta t = 0$ measured by illuminating the detector with spatially uniform incoherent X-rays is shown. Γ_D has been normalized to $<v^*>^2$, the square of the spatial average of v^*. The amplitude of the peak is $1+\frac{S^2_{\vec{q},v^*}}{<v^*>^2_{\vec{q}}}$, where $S^2_{\vec{q},v^*}$ is the spatial variance of v^*. A slice of the cross correlation function of two successive scans of the CCD detector is also shown with triangles, showing no correlation. When one needs to evaluate the speckle size, the cross correlation function has the advantage of removing the Poisson term in the right hand side of Eq. 5.6.

along the parallel transfer direction, here referred to as $q_{||}$. This explains why the width of the speckle contribution is different in the $q_\perp$ and $q_{||}$ directions in the inset of Fig. 5.4. If the detector is illuminated with a speckle pattern, $\Gamma(\vec{\Delta q},t,0)$ will contain a contribution due to the Poisson noise in the measured v^* coupled to the finite resolution of the detector, and one from the high contrast speckle pattern. To measure the speckle contribution, we must subtract this Poisson contribution from the detected correlation function, i.e.

$$\Gamma_s(\vec{\Delta q},t,0) = \Gamma(\vec{\Delta q},t,0) - \Gamma_D(<v^*>_{\vec{q}},\vec{\Delta q}), \tag{5.7}$$

where Γ_s is the speckle contribution. This treatment can be simplified further if we cross-correlate two successive speckle patterns, by approximating

$$\Gamma_s(\Delta\vec{q},t,0) \approx \Gamma(\Delta\vec{q},t,\Delta t) =< v^*(\vec{q},t)v^*(\vec{q}+\vec{\Delta q},t+\Delta t) >_{\vec{q}}, \tag{5.8}$$

where Δt is small compared to the time scale of any intensity fluctuations. In our case, this is a valid assumption since the dynamics is frozen for a sample at room temperature. Then the variance term in Eq. 5.6 due to Poisson noise disappears

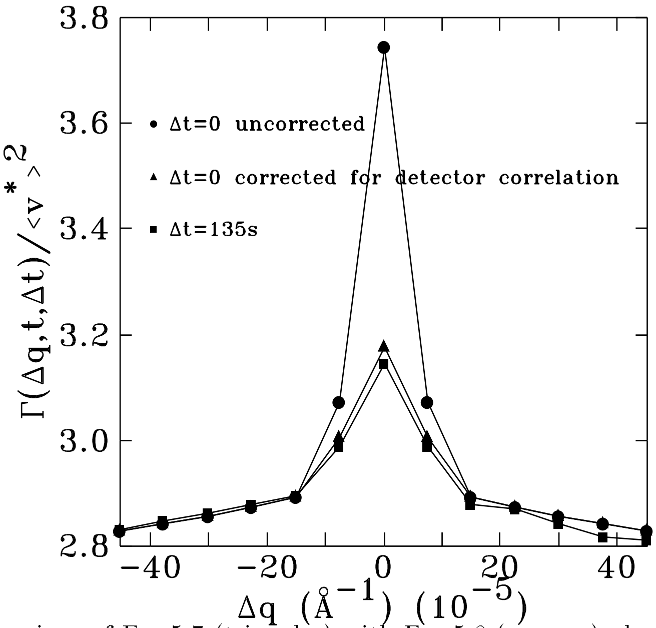

Figure 5.6: Comparison of Eq. 5.7 (triangles) with Eq. 5.8 (squares) along $2\Theta_{\|}$ for a static speckle pattern of Cu_3Au. The autocorrelation calculated from Eq. 5.5 is shown for comparison with circles. Note that the speckle pattern remains constant for 135 s since both equations yield the same Γ_s.

because $v^*(\vec{q},t)$ and $v^*(\vec{q},t+\Delta t)$ are independent. The treatment is also simpler since we do not need to take into account the Poisson contribution caused by the couplings between neighboring detectors, or pixels.

As shown in Fig 5.5, the cross correlation of two spatially uniform patterns does not show the excess correlation at $\Delta q = 0, \pm 1, \pm 2\ \Delta q_p$. There is no memory between different scans of the CCD detector. Furthermore, this tool is quite powerful in detecting any scattered beam motion. Fig. 5.6 shows the equivalence between Eq. 5.7 and Eq. 5.8. This also shows that the speckle pattern is unchanged after 135 s, which is a sign of good mechanical and optical stability of the experimental setup over this time period. Note that the Poisson and detector contribution in Eq. 5.7 could be also taken out by averaging the signal over N independent scans of the detector and then calculating Γ_s with

$$\Gamma_s(\vec{\Delta q},t,0) \approx <<v^*(\vec{q}+\vec{\Delta q},t)>_t<v^*(\vec{q},t)>_t>_{\vec{q}}. \tag{5.9}$$

In Eq. 5.6, the right hand side would then be divided by N because the error on a time average is reduced by $\sqrt{N}$, thus reducing the Poisson contribution.

Using Eq. 5.8, we can now estimate the speckle size in Fig. 5.1 and 5.2. If one assumes a point source illumination of the sample, the speckle size should be inversely proportional to the beam size. Fig 5.7 shows the crosscorrelation of two subsequent speckle patterns shown for different optical conditions. The correlation function was calculated using a window of 256 by 512 pixels which covers most of the data. Two effects are observed. As the pinhole diameter increases, the speckle size is reduced and the autocorrelation function becomes resolution limited. For example, for the wide open slits, the peak along $2\Theta_{||}$ subtends 9 points for the 3.5 μm pinhole but only 4 points for the 33 μm pinhole. Another indication of the resolution limit is seen for the data with narrow slits, since for $D = 15$ and 33 μm, the peak is the narrowest along $2\Theta_{\perp}$, the direction of high resolution on the CCD.

Another feature in Fig. 5.7 is the baseline shifts. For example, the crosscorrelation decays from a maximum of 2.9 to 2.6 for $D = 3.5$ μm (W), but decays from 3.93 to 3.6 for $D = 7.5$ μm (W). This baseline shift is caused by a change of the FWHM of the (100). This change of FWHM was measured by fitting the data to a two dimensional Gaussian later introduced in Eq. 5.11. It was found that the (100) is wider for smaller pinholes. For example, the fitted widths $\sigma_{||}$ and $\sigma_{\perp}$ decrease by 19 % when the input pinhole diameter is increased from $D = 3.5$ to 33 μm with wide open upstream slits. It is shown in section A.3 that the maximum of the spatial autocorrelation function for a two dimensional Gaussian representing the incoherent scattering is inversely proportional to the product of the fitted widths $\sigma_{\perp}$ and $\sigma_{||}$. In Fig. 5.8, the baseline of the correlation function, taken as the value of the crosscorrelation function along $2\theta_{\perp}$ after the decay due to speckle, is plotted versus the inverse of the product of the fitted widths. The baseline shift is proportional to $1/(\sigma_{\perp}\sigma_{||})$, in good agreement with the prediction found in Eq. A.35.

This dependence of the FWHM of the Cu_3Au (100) on the pinhole diameter D is very surprising. It is present in both data sets with open and closed upstream source slits. No coarsening dynamics occurred during this experiment since the sample was at 300 K. These measurements were performed with record incident and scattered wavevector resolutions. These measurements are micro-diffraction experiments on

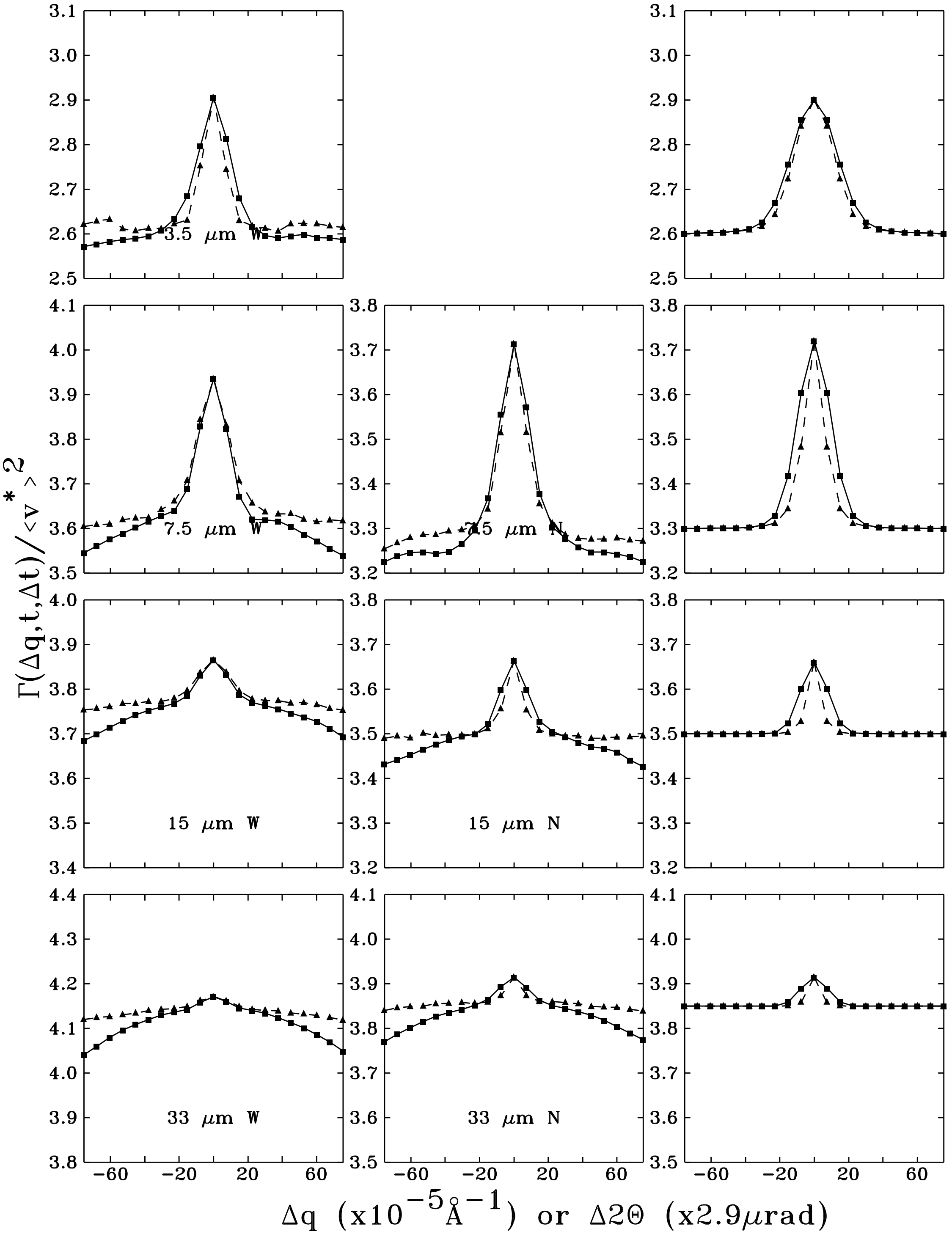

Figure 5.7: The effect of varying the collimating pinhole diameter, D, and the horizontal source size on the speckle size. The solid and dashed curves are respectively slices of the cross-correlation function between two subsequent exposures of the CCD along $2\Theta_{\parallel}$ and $2\Theta_{\perp}$ for wide (first column) and narrow source slits (second column). The speckle size increases as D is reduced for a given slit setting. Far away from $\Delta\vec{q} = 0$, the correlation function decays faster along $2\Theta_{\parallel}$ because the peak is narrower along this direction. The autocorrelation of a Fraunhofer diffraction pattern of a circular pinhole, convolved with the detector resolution is shown in the third column. The peak height and baseline were adjusted to match the values found in the data set with narrow slits along $2\theta_{\perp}$. The pinhole diameter varies from 3.5 to 33 μm, and slices along $2\Theta_{\perp}$ and $2\Theta_{\parallel}$ are shown respectively with dashed and solid lines. The spatial autocorrelation function of an ideal Fraunhofer diffraction pattern of the pinhole is in good agreement with the observed autocorrelation of speckle patterns for narrow slits.

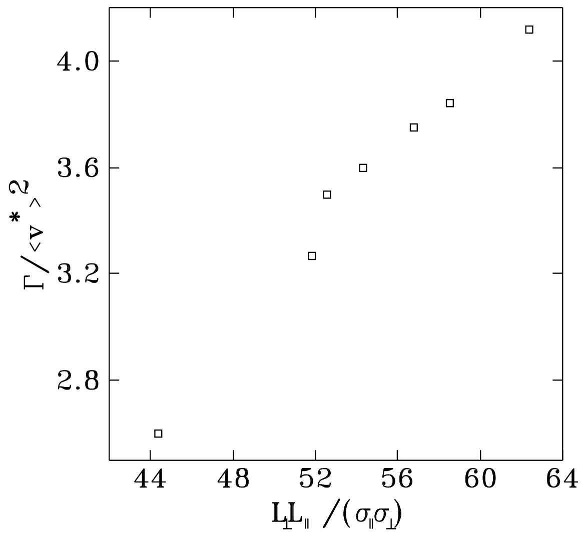

Figure 5.8: The inverse of the product of the fitted widths $\sigma_\perp$ and $\sigma_\parallel$ versus the maximum of the correlation function. $L_\perp$ and $L_\parallel$ are the dimensions of the rectangle in reciprocal space used to calculate the crosscorrelation function.

very small volumes of Cu_3Au. Since the FWHM decreases with increasing D, we speculate that by illuminating a larger volume of the sample, more large antiphase domains become fully illuminated. Therefore, a larger illuminated volume would better sample the *large domain tail* of the domain size distribution, resulting in a decrease of the average domain size measured by the FWHM of the peak.

This effect is reminiscent of another effect observed in single crystals of Cu_3Au and Fe_3Al. We have observed that by illuminating different parts of the sample with a given pinhole diameter[1], the intensity and FWHM of the superlattice peak varies. To optimize the scattering condition, we move the collimating pinhole over the crystal until a well ordered volume is found.

Since Sutton et al. [15] showed that the speckle size is proportional to the FWHM of the Fraunhofer diffraction pattern of a pinhole (see Eq 5.1), a natural way to understand the behavior of Fig 5.7 is to use the autocorrelation of the diffraction pattern of a pinhole as a theoretical estimate. The third column of plots in Fig. 5.7 shows the expected autocorrelation function of a Fraunhofer diffraction pattern of a circular pinhole, illuminated by a point source placed far away from the pinhole. The diffraction pattern was convolved with the detector resolution discussed in Chapter 3

[1]The collimating pinhole can be moved easily using two perpendicular high resolution Klinger motors.

and then autocorrelated. For large D, the speckle size is larger along $2\Theta_{||}$ than $2\Theta_{\perp}$, which implies that the speckle peak becomes resolution limited like the experimental data for narrow slits. The theoretical model better fits the data with narrow slits because the experimental condition is closer to the theoretical assumptions. Some differences between the data and theory are observed for $D = 3.5$ μm, where the measured correlation function for the data with wide open slits decays faster than the model. The measured data are narrower than the model. Perhaps some of this difference is caused by the fact that the Cu_3Au illuminated area is larger than the pinhole area since the sample is nearly outside the near-field diffraction of the 3.5 μm pinhole (see section 4.1).

The other noticeable effect is that closing the horizontal slits reduces the FWHM horizontally. For a given diameter D, slices along $2\Theta_{\perp}$ becomes narrower than those along $2\Theta_{||}$. This effect is small but does not depend on the method of calculation. The same result is also obtained using Eq. 5.9 on the data of Fig 5.2, or by cross correlating other sets of subsequent files. This is consistent with the FWHM of the diffraction pattern being input divergence limited when the slits are wide open, to becoming diffraction limited for narrow slits. The horizontal FWHM of the source image in the detector plane for wide slits, Δ_x, is approximately equal to $d_{sx}R_d/R_s$, where the horizontal FWHM of the source $d_{sx} = 0.91$ mm and the distance slit-pinhole $R_s = 17.3$ m. Here $\Delta_x = 55$ and 19 μm for wide and narrow slits respectively. Adding this geometrical optics effect to the FWHM of the diffraction pattern for a 7.5 μm pinhole shown in Eq. 4.4, gives an approximate FWHM of $55 + 24$ μm, and $19+24\mu$m for the wide and narrow slits respectively. This predicts a 45 % reduction of the FWHM of the speckle size by closing the horizontal slits. The measured reductions in the FWHM along $2\Theta_{\perp}$ in Fig. 5.2 are 20, 45 and 55 % reductions for the 7.5, 15 and 33 μm pinhole respectively. The difference between the measured and predicted change for the 7.5 μm pinhole may be caused by the resolution of the detector which has not been included in the calculation. Note that these effects will be easier to see in future experiments, by choosing a CCD array with finer resolution, or by placing the detector two or three meters away from the pinhole.

5.1.2 Contrast

We measure the contrast of the speckle pattern by

$$Ct(A, \vec{q}) \equiv \sqrt{\frac{S^2_{A,v^*}(\vec{q}) - <S^2_{t,v^*}>_A}{<v^*(\vec{q},t)>^2_A}}, \tag{5.10}$$

where the spatial variance $S^2_{A,v^*}(\vec{q})$ and mean $<v^*(\vec{q},t)>_A$ are evaluated at a given time, on a small area in q-space, A. The contrast might depend on the size of the area chosen, and on the average $\vec{q}$ vector at the center of A. For an ideal speckle pattern, one expects the contrast to be independent of the reciprocal space position. A very large window would increase the contrast artificially because the peak line shape varies across A. A very small window would poorly sample the spatial fluctuations. For the measurement shown next in Fig 5.9, a rectangular window with a width of 20 pixels along $2\Theta_{||}$ and height of 40 pixels covering approximately 25 % of the Cu_3Au peak FWHM was chosen to match the Cu_3Au peak asymmetry[1]. Using Eq. 5.3, with a detector area $A_s = (22.4\ \mu\text{m})^2$, one finds that the window chosen includes approximately 30 independent speckles for the 3.5 μm pinhole and 2700 for the 33 μm one. Thus for a given window size, we expect the standard deviation of the measured contrast for a small pinhole to be larger than for a large pinhole because one samples more independent speckles in the latter experimental condition.

In Eq. 5.10, $S^2_{t,v^*}(\vec{q})$, the variance calculated from a time sequence of measurements at $\vec{q}$, is a Poisson noise contribution subtracted from S^2_{A,v^*}. Because we do not expect any dynamics from the sample, S^2_{t,v^*} is due to counting statistics, incident beam intensity fluctuations and any electronic noise from the detector. With this definition, when the scattering is incoherent and no speckle is present, the contrast goes to zero since the spatial fluctuations should be equal to the spatial average of the time fluctuations in Eq. 5.10.

Fig. 5.9 shows the speckle pattern contrast for various pinhole diameters and two upstream horizontal slit settings shown in Fig 5.2. The contrast increases as D

[1] A square window of 20×20 pixels gave similar results.

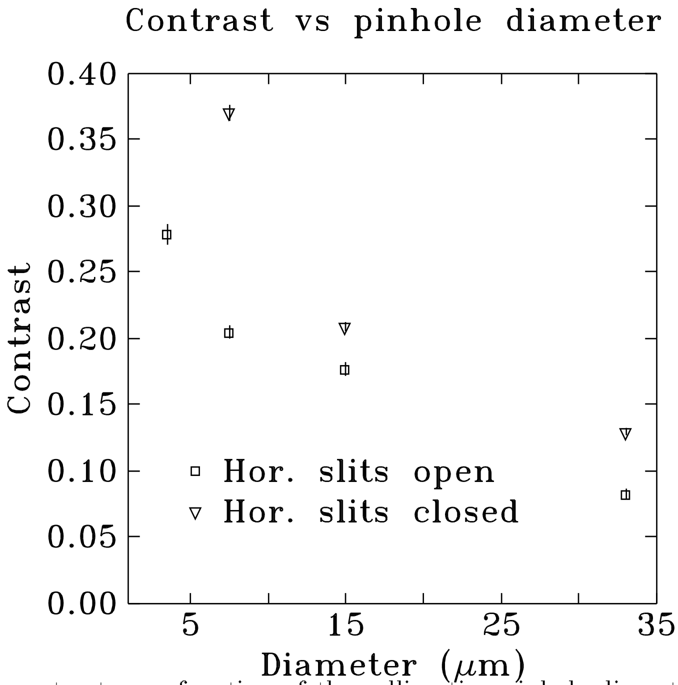

Figure 5.9: The contrast as a function of the collimating pinhole diameter D, as computed from Eq. 5.10. Two data sets are shown for open horizontal slits (2mm) and closed horizontal slits (0.31mm). Closing the horizontal slits increases the contrast for a given D because it increases the horizontal coherence length l_x.

is reduced, and increases as l_x is increased. This is consistent with the statistical properties of speckle. Note also that the contrast in Fig. 5.9 is proportional to the amplitude of the decay of the crosscorrelation function in Fig. 5.7. For example, for $D = 3.5$ μm (W), the crosscorrelation in Fig. 5.7 decays from a maximum of 2.9 to 2.6, thus $\sqrt{(2.9-2.6)/2.6} = 0.34$, which compares reasonably well with a contrast of 0.28 found in Fig. 5.9.

The measured contrast for Cu_3Au seems lower than expected. The contrast for an ideal speckle pattern is one. Let us calculate, for example, the contrast for $D =$ 7.5 μm, and closed horizontal slits. At NSLS, the vertical coherence length is much larger than D. The horizontal transverse coherence length is $l_x = \lambda R_s/2d_s$, where R_s is 17.3 m, $\lambda = 1.797$ Å, and $d_s = 0.31mm$. Here $l_x = 5$ μm is smaller than the pinhole diameter D, thus some contrast is lost in the horizontal. One expects the contrast to drop from one to $\approx \sqrt{l_x/D} = 0.82$. In Cu_3Au, the longitudinal coherence condition is satisfied, so no contrast should be lost. Another loss of contrast will be caused by averaging many speckles in a detector area. Using Eq. 5.3, the number